ADVANCES IN ATMOSPHERIC SCIENCES, VOL. 35, JUNE 2018, 723–736

• **Original Paper** •

Modeling the Warming Impact of Urban Land Expansion on Hot Weather Using the Weather Research and Forecasting Model: A Case Study of Beijing, China

Xiaojuan LIU[1], Guangjin TIAN[*1,2], Jinming FENG[3], Bingran MA[1], Jun WANG[3], and Lingqiang KONG[1]

[1]*State Key Laboratory of Water Environment Simulation, School of Environment, Beijing Normal University, Beijing* 100875*, China*

[2]*School of Government, Beijing Normal University, Beijing* 100875*, China*

[3]*CAS Key Laboratory of Regional Climate-Environment for Temperate East Asia, Institute of Atmospheric Physics, Chinese Academy of Sciences, Beijing* 100029*, China*

(Received 31 May 2017; revised 15 November 2017; accepted 29 November 2017)

ABSTRACT

The impacts of three periods of urban land expansion during 1990–2010 on near-surface air temperature in summer in Beijing were simulated in this study, and then the interrelation between heat waves and urban warming was assessed. We ran the sensitivity tests using the mesoscale Weather Research and Forecasting model coupled with a single urban canopy model, as well as high-resolution land cover data. The warming area expanded approximately at the same scale as the urban land expansion. The average regional warming induced by urban expansion increased but the warming speed declined slightly during 2000–2010. The smallest warming occurred at noon and then increased gradually in the afternoon before peaking at around 2000 LST—the time of sunset. In the daytime, urban warming was primarily caused by the decrease in latent heat flux at the urban surface. Urbanization led to more ground heat flux during the day and then more release at night, which resulted in nocturnal warming. Urban warming at night was higher than that in the day, although the nighttime increment in sensible heat flux was smaller. This was because the shallower planetary boundary layer at night reduced the release efficiency of near-surface heat. The simulated results also suggested that heat waves or high temperature weather enhanced urban warming intensity at night. Heat waves caused more heat to be stored in the surface during the day, greater heat released at night, and thus higher nighttime warming. Our results demonstrate a positive feedback effect between urban warming and heat waves in urban areas.

Key words: heat wave, numerical simulation, urbanization, surface heat flux, WRF, UCM

Citation: Liu, X. J., G. J. Tian, J. M. Feng, B. R. Ma, J. Wang, and L. Q. Kong, 2018: Modeling the warming impact of urban land expansion on hot weather using the Weather Research and Forecasting model: A case study of Beijing, China. *Adv. Atmos. Sci.*, **35**(6), 723–736, https://doi.org/10.1007/s00376-017-7137-8.

1. Introduction

Urbanization, particularly urban land expansion (Feng et al., 2014), is one of the most important anthropogenic factors influencing regional climate change (Kalnay and Cai, 2003; Zhou et al., 2004; Sun et al., 2014, 2016). For example, the urban heat island (UHI) effect is an urbanization-driven phenomenon reported by many studies (Kalnay and Cai, 2003; Zhou et al., 2004; Wang et al., 2017a). Urbanization increases water-impervious surfaces, solar radiation absorption, and heat storage, while decreasing evapotranspiration (Oke, 1982). This ultimately leads to surface air temperature increases in urban areas.

China has undergone rapid urbanization and dramatic economic development since its reform policies in late 1978 (Chen, 2007; Fang et al., 2016). Beijing, the capital of China, has been undergoing a rapid urbanization process over the past three decades, as villages and farmlands are increasingly replaced by high-rise buildings. Its population is higher than those of some Asian countries and it is one of the most urbanized cities in China (Xie and Cao, 1996; Yan et al., 2010). By 2013, 53.73% of China's population was urban, while that of Beijing was 86.3%—the highest proportion in China except Shanghai (89.60%) (National Bureau of Statistics PRC, 2014). The impacts of this expansion on the summer weather and climate in Beijing are drawing increasing attention from observational and simulation studies (Miao et al., 2009; Wang et al., 2013a). Models are commonly applied in regional climate simulations and are a critical method with which to study such changes because they can improve the spatial resolution of regional climate over measurements taken across a network of meteorological stations (Chen et al., 2004). Previous studies have generally used two-year urban land datasets

* Corresponding author: Guangjin TIAN
Email: tianguangjin@bnu.edu.cn

(Wang et al., 2013b; Cui et al., 2015), or combined non-urban scenarios and one-year urban land datasets to perform sensitivity tests (Miao et al., 2009; Feng et al., 2012). However, these do not capture the evolution of air temperature at different stages of urban land expansion. Identifying how changes in air temperature are driven by urbanization has clear practical implications for urban planning and ameliorating the UHI effect.

Anthropogenic influences have increased the probability of extreme weather events, such as the European heat wave of 2003 and the Russian heat wave of 2010 (Stott et al., 2004; Field et al., 2012; King et al., 2015). These extreme heat events contributed to a series of social and economic problems, including power shortages and human health impacts (Hales, 2015; King et al., 2015). It is worth noting that extremely hot weather or heat waves can even lead to mortality in metropolitan areas (Hales, 2015). Most previous studies modeling the impacts of urbanization on air temperature have generally made a separate analysis of heat waves and longer-term effects (Stott et al., 2004; Meng et al., 2011; Chen et al., 2014; Wang et al., 2017a). Moreover, there is a lack of comparability between these separate studies of heat waves and longer-term effects because of the differences in research methods (Wang et al., 2013b; Zhang et al., 2011). Therefore, the impact of urban land expansion on both heat waves and longer periods of hot weather should be explored, helping us to build an understanding of the different urban-induced temperature changes under various periods of weather conditions.

In this study, we used the mesoscale Weather Research and Forecasting (WRF) model coupled with a single urban canopy model (UCM) and high-resolution land cover datasets from three stages of urbanization to simulate the near-surface air temperature in summer 2010 in Beijing, China. The objectives of the study were to: (1) analyze the spatial and temporal patterns of summertime urban warming influenced by three stages of urban land expansion during 1990–2010 across Beijing and explore the mechanisms based on the surface energy balance; and (2) analyze the impacts of heat waves and high temperature weather on urban-induced warming and the mechanisms associated with the surface energy balance, and reveal the interrelationship between urban-induced warming and heat waves.

2. Methods

2.1. *Model configuration*

We used the WRF model (version 3.7.1) coupled with a single-layer UCM (SLUCM) to simulate 2-m air temperature in this study. The WRF model is a numerical weather prediction and atmospheric simulation system designed for both research and operational applications (Skamarock et al., 2008). The simulation results obtained using the WRF model have a higher spatial resolution compared with measurements based on meteorological stations (Chen et al., 2004, 2014). Coupling it with an SLUCM allows for a better description of the physical processes associated with the exchange of momentum, heat, and water vapor near the surface of urban environments (Tewari et al., 2007). The SLUCM used in this study was a single-layer model with some simplified urban geometry parameters and corresponding calculations, such as shadowing from buildings, reflection of short- and longwave radiation, the wind profile in the canopy layer, and thermal conduction equations for roofs, walls, and road surfaces (Kusaka et al., 2001; Kusaka and Kimura, 2004; Tewari et al., 2007). The coupled mesoscale atmospheric–urban modeling system thus has considerable potential to reproduce urban effects. Previous studies have shown that such a model configuration (i.e., WRF/SLUCM) can precisely simulate regional urban climate (Cao et al., 2016; Kusaka et al., 2012; Feng et al., 2012).

In this study, three one-way nested domains (D01, D02 and D03) were set up in the WRF simulation (Fig. 1a). The grid points for D01, D02 and D03 were 66×66, 121×121 and 191×191, with grid spacings of 25, 5, and 1 km, respectively. The coarse domain was centered at (40.10°N, 116.50°E) with a Lambert conformal conic map projection. The main physics parameterization schemes included the WRF single-moment 3-class scheme (Hong et al., 2004), the rapid radiative transfer model for general longwave radiation scheme (Mlawer et al., 1997), the Dudhia scheme for shortwave radiation (Dudhia, 1989), the Yonsei University planetary boundary layer (PBL) scheme (Hong et al., 2006), the Kain–Fritsch cumulus parameterization (Kain, 2004), and the Noah land surface model (Chen and Dudhia, 2001), coupled with the SLUCM (Kusaka et al., 2001). To identify the responses of meteorological factors to land use change, human-induced anthropogenic heat was not considered in our simulation. In general, the simulated near-surface meteorological factors can be impacted by the number of vertical levels, especially within the PBL. To further validate the impact on 2-m air temperature, four vertical levels within the PBL (9, 12, 15 and 18 levels) were tested in the study region. The results showed that when the number of vertical levels within the PBL increased by one, the regional-averaged (and station-averaged) 2-m air temperature simulated by WRF basically reduced by ~ 0.01°C–0.02°C. Because this impact was relatively small, 30 full sigma levels from the surface up to 50 hPa and approximately nine levels below 1.5 km in the vertical direction were used in the subsequent analyses.

2.2. *Initial and boundary conditions*

We chose the summer (June–August) in 2010 as the synoptic background. It included a heat wave, from 2 to 8 July 2010 (Sun et al., 2016). According to the Beijing Statistical Yearbook (http://www.bjstats.gov.cn/tjsj/), the maximum recorded temperature on 5 July 2010 was 40.6°C, which was the highest temperature in Beijing in early July since 1951. We used the daily datasets from 17 meteorological stations in Beijing to calculate the station-averaged observed temperature during three time periods (Fig. 2). These three periods included the day of 5 July 2010 (hereafter, EH), the heat wave of 2–8 July 2010 (including the EH; hereafter, HW),

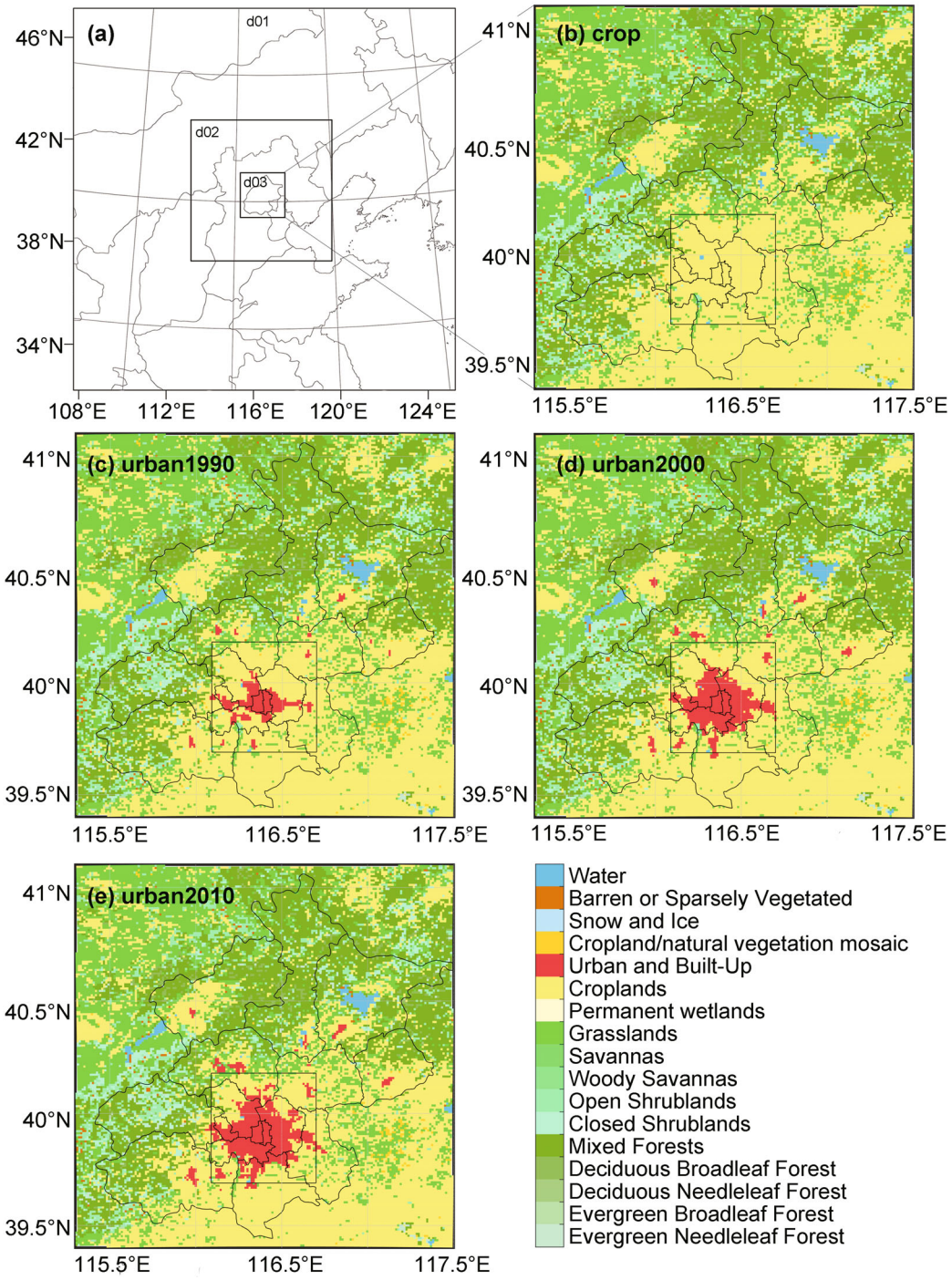

Fig. 1. (a) The three one-way nested domains used for the WRF/SLUCM numerical simulation and (b–e) the Beijing land use data for (b) cropland (hypothetical scenario), (c) urban and built-up land in 1990, (d) urban and built-up land in 2000, and (e) urban and built-up land in 2010. The resolution is 1 km. The frame indicates the "six-ring" area of Beijing.

and the summer (June–August) in 2010 (including the HW; hereafter, JJA). It was clear that the observed near-surface air temperature in HW was significantly higher (~ 5°C–8°C) compared to the whole summer. The difference between HW and EH was relatively low because of their similar synoptic backgrounds (observed air temperature for HW was ~ 2°C higher than that for EH, except for daily minimum temperature).

The initial and boundary conditions for 27 variables were from the NCEP-FNL data at 6-h increments. The variables included air temperature, geopotential height, land cover, sea level pressure, soil moisture/water content, surface winds, and upper level winds. The case simulations in WRF were initiated at 0000 UTC 24 May and ran until 0000 UTC 1

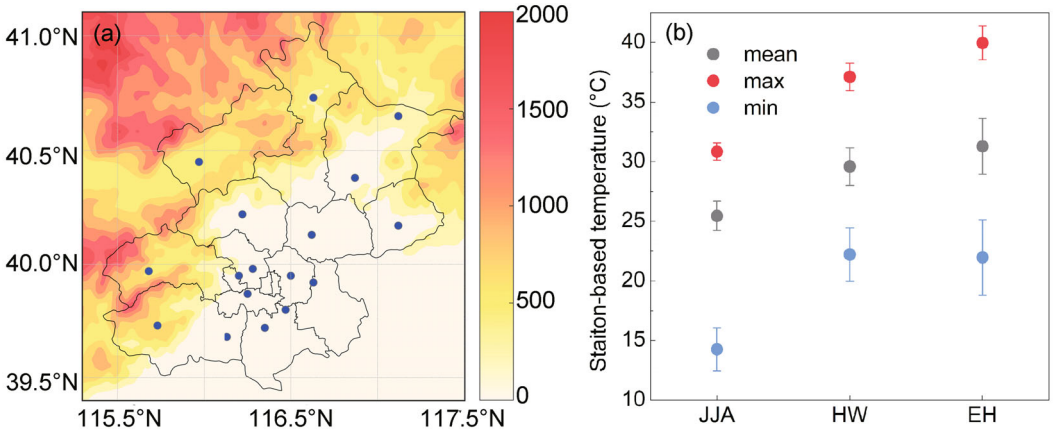

Fig. 2. (a) The locations of the meteorological stations in Beijing. The shaded contours represent the terrain height (units: m). The irregular black lines indicate the administrative boundaries of the city. (b) Station-averaged observed daily mean (mean), maximum (max) and minimum (min) air temperatures during the three time periods (JJA, HW and EH) of this study. The error bars represent the standard deviations above and below the station-based mean.

September. The first eight days were considered as the spin-up time and not used for the final analysis.

2.3. *Land use data*

The urban expansion process in Beijing can be divided into three stages: (1) 1990–1995, when urban development was in a state of spontaneous expansion, and the urban land area increased from 989.62 km^2 in 1990 to 1465.10 km^2 in 1995; (2) 1996–2000, when urbanization slowed due to government intervention; and (3) 2000–2008, when urban development shifted due to macro-level control by the government, and the urban land area increased from 2049.4 km^2 in 2004 to 3377.15 km^2 in 2008. Following the stages outlined above, we used three periods of urban land use data (1990, 2000 and 2010) developed by the Institute of Geographical Sciences and Natural Resources Research of the Chinese Academy of Sciences using Landsat TM and Landsat ETM scenes (IGSNRR, http://www.igsnrr.ac.cn) to update the 20-class MODIS land cover dataset in WRF. The spatial patterns of urban land use data with 1-km resolution are presented in Figs. 1c–e. To assess the surface air temperature changes induced by urban land expansion, we also provide a hypothetical land use scenario (referred to as "crop" in Fig. 1b), with the grids replaced by nearby land use types (mostly cropland).

2.4. *Experimental design*

To simulate how urban land expansion influenced the summer temperature at different stages of land use during 1990–2010, we used WRF/SLUCM to conduct the following sensitivity experiments: (1) "Crop"—a hypothetical land use scenario with the grids replaced by nearby land use types; (2) "Urban1990"—land use data from 1990; (3) "Urban2000"—land use data from 2000; and (4) "Urban2010"—land use data from 2010. Except for the urban land cover data, the same experimental conditions were used in all tests. The Urban2010 simulation was considered as the control run because the urban land information best matched the simulated time. The differences between urban2010/urban2000/urban1990 and the crop scenario represented the urban warming induced by the three stages of urban land expansion in 1990–2010.

2.5. *Observations*

To validate the model in this study, we used (1) the normalized daily dataset from 17 meteorological stations in Beijing (Fig. 2a) from June to August 2010; (2) the gridded, monthly temperature observations with a spatial resolution of 0.5° × 0.5° (V2.0) from June to August 2010; and (3) the hourly dataset during 2–8 July 2010 from Beijing meteorological station (39.80°N, 116.47°E). All datasets were provided by the National Climate Center of the China Meteorological Administration (http://data.cma.cn/).

3. Results and discussion

3.1. *Model evaluation*

To evaluate the model, we compared the simulated results with direct observations from the corresponding period. According to the locations of the 17 meteorological stations, we calculated the station-averaged simulated results in JJA (control run). The statistics showed that the model tended to overestimate the mean temperature, with a systematic bias of 1.14°C (Table 1), which was at least as good as what had been shown in prior studies [1.55°C in Wang et al. (2013b); 1.55°C in Wang et al. (2015a); 1.0°C–1.5°C in Cao et al. (2016)]. Previous studies attributed the positive systematic discrepancies to the inaccuracies of the boundary conditions and sensitivities of the physics parameterization schemes (Cao et al. (2016); Wang et al. (2015a)). In this study, the warm bias of the temperature would have been primarily caused by the simulation without consideration of atmospheric aerosol. This is because atmospheric aerosol can reduce the fraction

Table 1. Comparison of the simulated and observed station-averaged near-surface air temperature in JJA. OBS, observation; SIM, simulation; BIAS, SIM minus OBS; N-SD, normalized standard deviation; SCC, spatial correlation coefficient (** for $P < 0.01$). Units: °C.

	MEAN		SD					
	SIM	OBS	SIM	OBS	BIAS	N-SD	RMSE	SCC
Mean	26.63	25.49	1.61	1.26	1.14	1.28	1.28	0.94**
Max	41.22	40.18	1.90	1.22	1.03	1.56	1.67	0.71**
Min	14.11	14.34	1.85	1.82	−0.22	1.02	1.23	0.78**

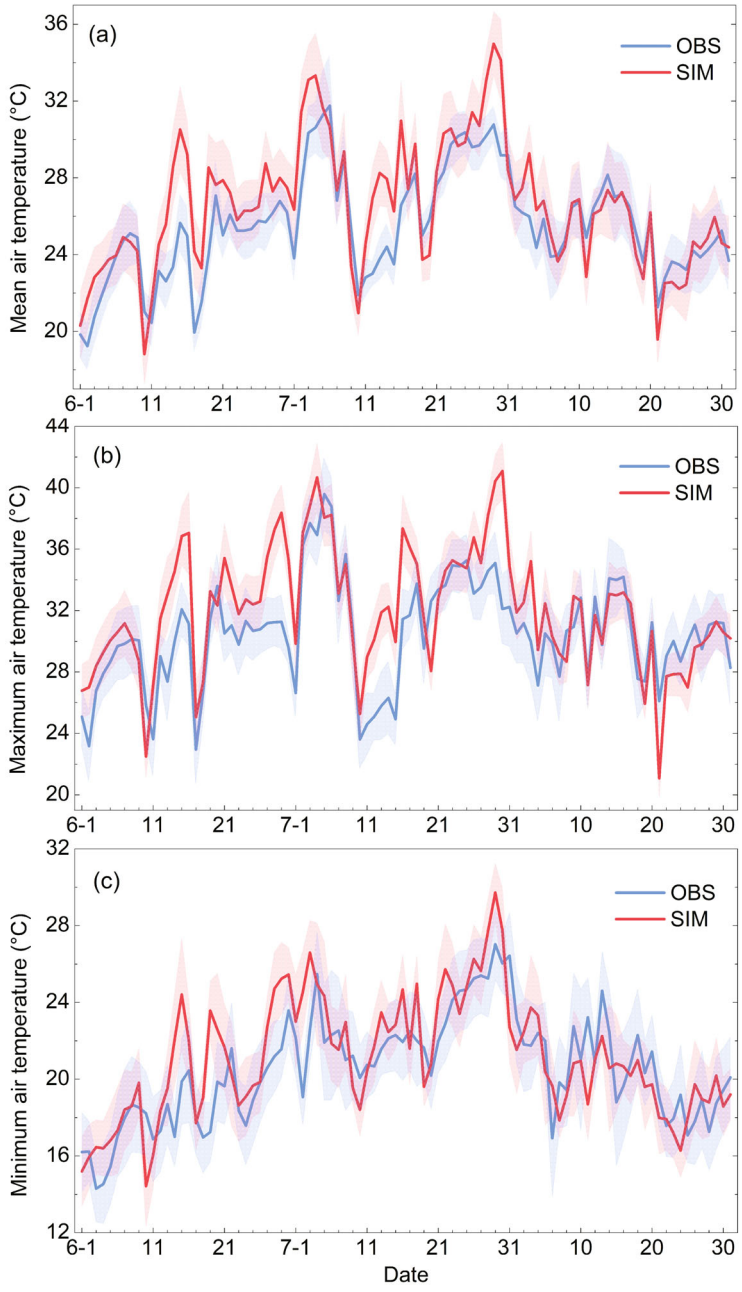

Fig. 3. Comparison of station-averaged daily (a) mean, (b) maximum and (c) minimum air temperature in JJA 2010 between observations (OBS) and the WRF simulation (SIM). The shaded areas (blue/red) represent the standard deviation above and below the mean. SIM is the simulated result of the control run (urban2010).

of solar shortwave radiation arriving at the surface, reduce the ground-stored heat, and accordingly decrease the air temperature. The station-based spatial correlation of mean temperature between the observations and simulated data was 0.94 ($P < 0.01$). The model also overestimated the observed maximum air temperature, with an absolute error of ~ 1°C (Table 1). Its station-based spatial correlation (0.71) was smaller than that of the mean and minimum temperature. The simulated minimum air temperature agreed well with the observed data, with an absolute error of ~ 0.2°C (Table 1). Figure 3 indicates that the temporal evolution of the simulated daily temperature agreed with observations.

We also compared the observed and simulated hourly air temperature during HW (2–8 July 2010) at Beijing meteorological station (Fig. 4). The simulated air temperature during these seven days was generally consistent with observations, especially on 2, 3 and 8 July. The model generally underestimated the nighttime temperature. Moreover, it underestimated the air temperature throughout almost the entire duration of EH. The spatial distributions of summer mean temperature in Beijing for the simulation and observations are examined in Fig. 5. Although the $0.5° \times 0.5°$ gridded spatial observational dataset could not validate our high-resolution simulated data well, the spatial pattern of the simulated near-surface air temperature was comparable to that of the observational data. The summer-averaged air temperature in Beijing increased gradually from northwest to southeast. The simulated temperature was largely consistent with observations, indicating that the model is generally able to capture the spatial pattern of mean air temperature in Beijing. Note that we only focused on the differences in near-surface air temperature between urban2010/urban2000/urban1990 and the crop scenario in our study. Therefore, the simulated systematic bias would be offset by calculating the differences among scenarios.

3.2. *Impacts of urban land expansion on summer near-surface air temperature*

We investigated the response of 2-m air temperature in summer to urban land expansion in 1990–2010 based on the

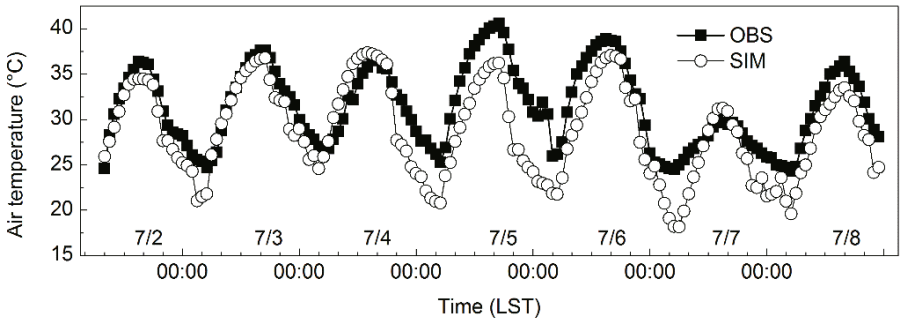

Fig. 4. Comparison of hourly air temperature from 0800 LST 2 July to 2300 LST 8 July 2010 between observations (OBS) and the WRF simulation (SIM) at Beijing station (39.80°N, 116.47°E).

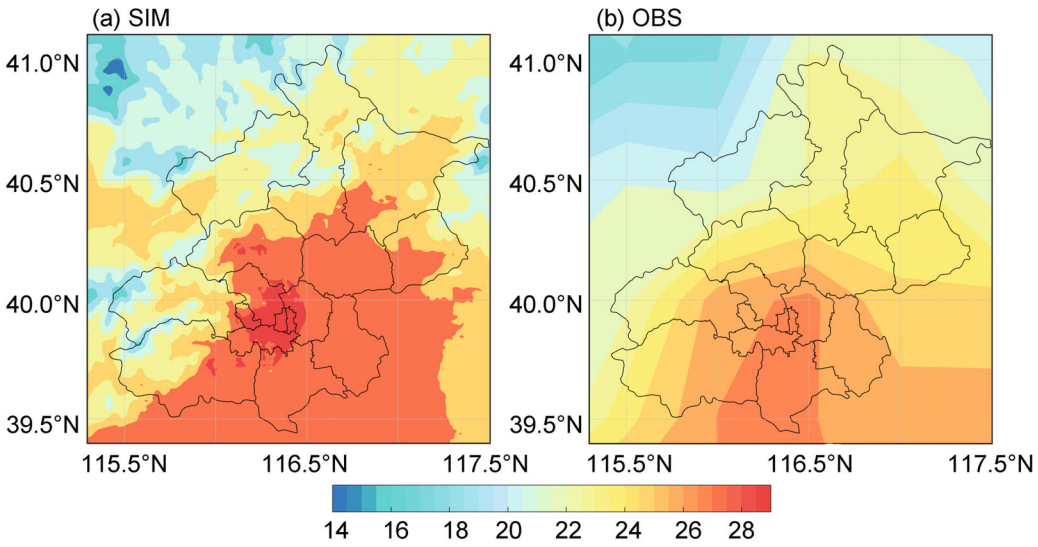

Fig. 5. Comparison of (a) WRF-simulated (SIM) and (b) observed (OBS) temperature spatial distributions during JJA (units: °C).

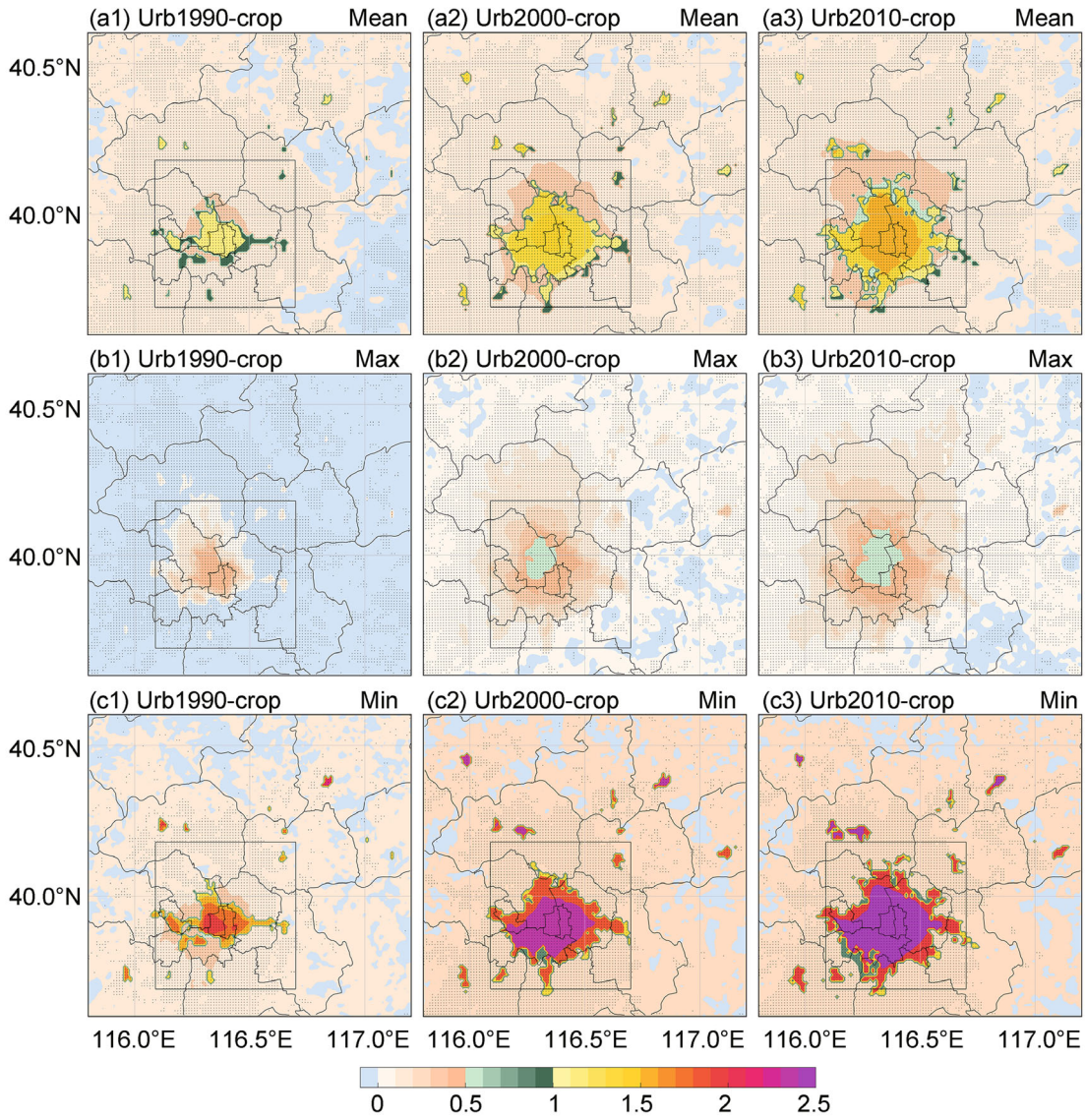

Fig. 6. Summer-averaged spatial patterns of the difference in daily 2-m (a) mean, (b) maximum and (c) minimum temperature between the three urban land datasets (urban1990, urban2000, and urban2010) and the crop scenario (units: °C). Black dots represent significant differences in July (> 99% probability) between paired samples based on the pairwise *t*-test. The black frame indicates the six-ring area of Beijing.

WRF simulations using four land use scenarios. Figure 6 shows the spatial changes in 2-m air temperature between the three urban land use scenarios and the crop scenario. The spatial characteristics of the warming area's expansion approximately matched the evolving horizontal sizes of urban land use during 1990–2010 (Fig. 1). It also implied a "ring of spread" feature corresponding to the urban land expansion in Beijing in 1990–2010, which is consistent with the result reported by Jacobson et al. (2015). By 1990, the mean 2-m air temperature had increased by 1.04°C on average over the urban grids in Beijing, and the most significant spatial warming was 1.23°C. The warming area was primarily distributed at the center of Beijing (Fig. 6a1). By 2000, the warming area had expanded from the center of Beijing to the surroundings (Fig. 6a2), while the warming increased by 0.2°C over the urban grids in 2000. By 2010, the warming area had continued to spread in all directions, especially in the northerly direction (Fig. 6a3), while the warming averaged over urban grids in 2010 had an additional 0.06°C, as compared to that in 2000. The warming caused by urbanization in 2010 was slightly higher than the result reported by Wang et al. (2012) for the Beijing–Tianjin–Hebei (BTH) urban agglomeration, which demonstrates the reasonability of our result because of the overwhelming urbanization in Beijing. Urban warming increased with urban land expansion but its increment decreased slightly with time. That is, the regional average warming speed induced by urban land expansion declined. A possible reason for this is that the area growth rate of urban land was moderated after 2000.

Due to the different urban areas for the three urban devel-

opment periods, the regional statistical results above only indicated the warming intensities over urban areas of the three periods. For a better explanation of the impacts of urbanization, we calculated the regional average warming in the "six-ring area" of Beijing (The region was indicated by the black frame in Fig. 6). The results indicated that the regionally averaged 2-m mean air temperature in the 1990, 2000 and 2010 urbanization periods was 0.23°C, 0.50°C and 0.64°C higher, respectively, than the crop scenario. This also demonstrated the relatively slow urban warming during 2000–2010. The impact by urbanization in 2010 (0.64°C) was higher than the result of 0.28°C reported in Wang et al. (2012) because our research area was concentrated in the urban grids (the six-ring area). This suggests that the regionally averaged warming over the six-ring region has grown by an average of ~ 0.2°C $(10\ \mathrm{yr})^{-1}$, which is roughly consistent with the observed result reported in Yan et al. (2010).

We found a smaller warming signal for 2-m maximum air temperature, and the warming primarily spread in the northerly direction (Fig. 6b). The largest change in maximum air temperature in the 1990, 2000 and 2010 urbanization periods was 0.41°C, 0.62°C and 0.64°C, respectively. The differences in 2-m minimum air temperature were drastic between the three land use periods and the crop scenario (Fig. 6c). The largest spatial increment in 2-m minimum air temperature in Beijing was 2.27°C, 2.39°C and 2.46°C, respectively. Urban warming was higher for daily minimum air temperature than for daily maximum, as reflected in previous studies (Miao et al., 2009; Chen et al., 2014; Wang et al., 2017a).

We investigated the diurnal cycle of urban warming in summer averaged over the six-ring area of Beijing (Fig. 7a). Daytime warming remained small (< 0.2°C) during 0900–1600 LST, and the smallest warming for the three periods of urban land expansion occurred at 1200 LST. The warming gradually increased in the afternoon and peaked at ~ 2000 LST—the time of sunset. The warming decreased slowly at nighttime and began to weaken rapidly after 0500 LST. Note that urban warming at night was nearly constant (the warming decreased < 0.1°C, approximately, during 2000–0500 LST), which was in keeping with observations for Beijing reported by Wang et al. (2017b). Based on the features of the diurnal cycle, the nocturnal average warming intensity was about three times that in the daytime for the three urbanization periods.

Change in near-surface air temperature results from the surface energy balance, which can be expressed by the following formula when the anthropogenic heat flux is not considered (Oke, 1982):

$$R_{\mathrm{n}} = H + \mathrm{LE} + G\,, \tag{1}$$

where R_{n} is the net all-wave radiation, H is the sensible heat flux, LE is the latent heat flux, and G is the ground heat flux (the heat storage). Figure 8 shows the diurnal cycle of the urban-induced changes in surface heat flux averaged over the six-ring area of Beijing. The changes in surface heat flux in 2000–2010 were smaller than in 1990–2000, which was consistent with the evolution of temperature change. The net radiation increased during the day because of the larger amount of solar radiation trapped by the urban surface. Negative net radiation emerged at night because of the relatively high nocturnal longwave emissions from the urban surface (Fig. 8a). Urbanization led to more surface heat stored in the day, and then a greater release at night (Fig. 8d). The latent heat flux decreased notably during the day because of lower soil evapotranspiration and less standing water over urban land (Douglas et al., 2006). Another reason was the low fraction of vegetation (hence, low evapotranspiration) in the urban areas. When cropland is converted to urban land, soil

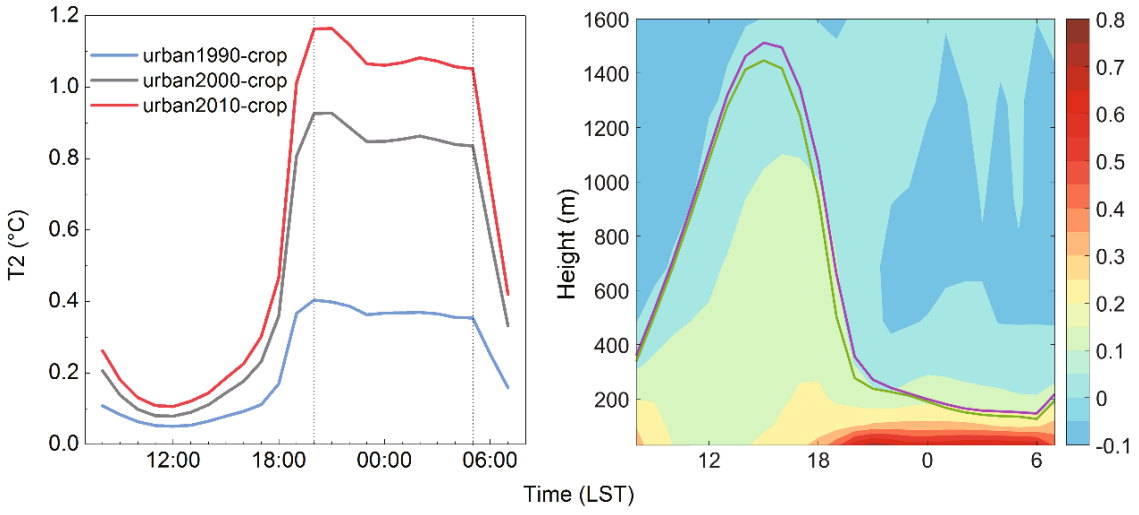

Fig. 7. (a) Summer-averaged diurnal cycle of the difference in 2-m air temperature averaged over the six-ring area of Beijing between the different urban development periods and the crop scenario. Two vertical dotted lines indicate sunset (2000 LST) and sunrise (0500 LST), respectively. (b) Time–height cross section of air temperature change in the lower atmosphere (color-shaded; urban2010 minus the crop run; units: °C). The purple (green) line shows the summer-averaged diurnal cycle of PBL height over the six-ring area for the urban2010 (crop) run.

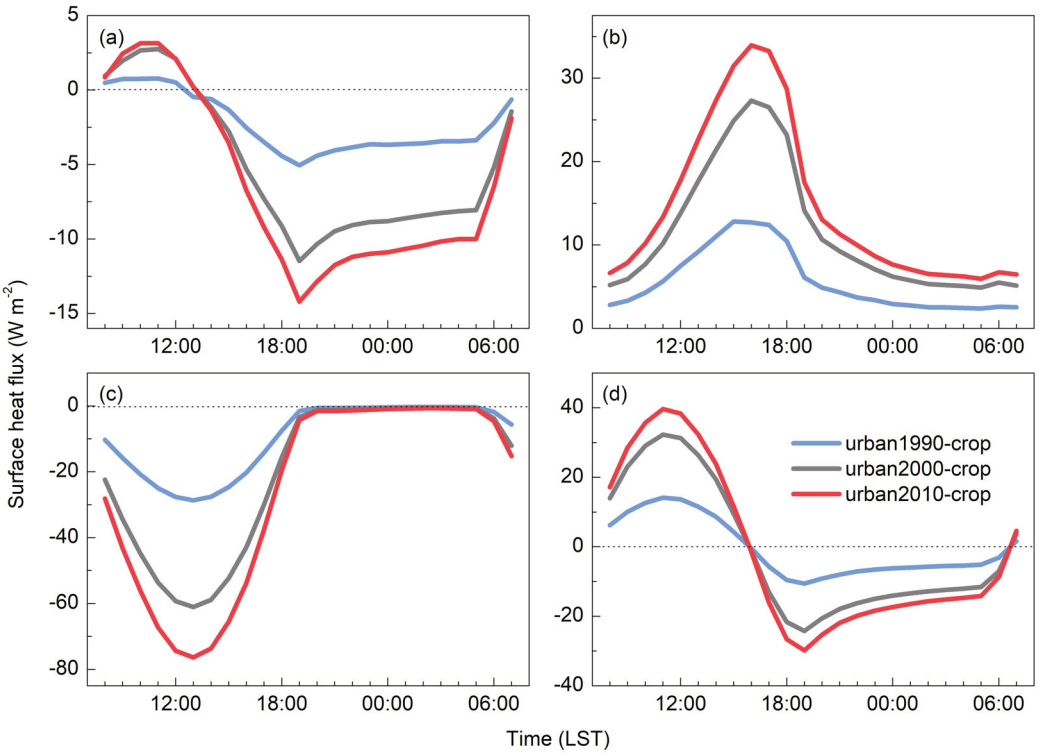

Fig. 8. Summer-averaged diurnal cycle of the difference in surface heat flux averaged over the six-ring area of Beijing between the different urban development periods and the crop scenario: (a) net radiation flux; (b) sensible heat flux; (c) latent heat flux; (d) ground heat flux.

moisture reduces notably (Jacobson et al., 2015), which results in a decrease in daytime soil evapotranspiration. There was little difference in nighttime water evapotranspiration between the urban and crop areas. Water evaporation is mainly influenced by the wind and the difference in vertical water vapor. In the daytime, the higher surface temperature led to a greater difference between the surface and near-surface vertical water vapor in the urban areas. In addition, the wind speed in the day was generally larger and the aerodynamic resistance was smaller than that at night. So, these aspects explained the diurnal variation of changes in latent heat flux. Therefore, the changes in latent heat flux were close to zero after 2000 LST (around sunset) (Fig. 8c).

During the day, the significant changes in latent heat flux resulted in more sensible heat flux from the surface layer to the air (Fig. 8b). The urban land expansion resulted in more heat being stored in the urban surface during daytime and more heat being released at night, which caused urban warming at night. However, compared to the urban-induced change in latent heat flux in the daytime, the change in ground heat flux was relatively small. According to the surface energy balance [Eq. (1)], with small net radiation the increase in sensible heat flux in the daytime would have been mainly attributable to the change in latent heat flux. Due to greater changes in latent heat flux in the day compared to those in ground heat flux at night, greater changes in sensible heat flux occurred in the day. Therefore, the changes in sensible heat flux peaked at around 1500–1600 LST, which directly contributed to urban warming (Fig. 7a).

The release of stored heat led to the small increase in sensible heat flux at night (Fig. 8b). However, the urban warming at night was higher than that in the day, although the nighttime increment in sensible heat flux was smaller. One reason for this was the impact of the diurnal cycle of PBL height (Fig. 7b). The PBL stratification was unstable during the day due to the increase in sensible heat flux, triggering strong vertical turbulent mixing (Wang et al., 2017a). Moreover, the warming was distributed to suburban areas due to the active advection in the boundary layer, which might reduce daytime warming intensity in urban areas (Wang et al., 2015b). At nighttime, the smaller surface heat flux led to a reduction in turbulent kinetic energy, further leading to the stable PBL stratification (the shallower PBL at night; Fig. 7b). Hence, urban-induced surface heat at night was not easily released, and the urban-induced warming was intensified within the shallow PBL. Therefore, the higher nighttime warming was formed. In addition, the daytime solar radiation between urban and crop areas differed little. However, the nighttime longwave radiation was larger in urban areas because of the high amounts of storage and slow release of urban heat, which caused the obvious urban warming at night (Wang et al., 2015b).

The diurnal cycle of urban warming showed a very small warming in the day and a near constant warming effect at night in Beijing (Fig. 7a), which is different from that in eastern China reported by previous studies (Chen et al., 2014;

Wang et al., 2017a). In Beijing, the soil moisture in the urban and crop areas differed little because the summer climate in Beijing is drier than that in eastern China. Thus, the magnitude of urban-induced change in latent heat flux would be small in Beijing, leading to the small urban warming in the day. The urban warming intensity at night was generally attributable on the one hand to the urban-induced changes in sensible heat flux, whilst on the other hand to the diurnal variation of the PBL height. In addition, due to the smaller increment in sensible heat flux at night and its maximum in the day, the shallower PBL was likely the major reason for the larger urban-induced warming at night. The change in sensible heat flux at night resulted from the release of surface stored heat. If the PBL height is constant after sunset, urban warming intensity will decrease exponentially. In fact, however, the PBL height decreased gradually after 1500 LST (Fig. 7b), which slowed down the reduction process of warming intensity at night. Therefore, the near constant warming effect at night was formed when the nighttime variations of PBL height (Fig. 7b) and the urban-induced change in sensible heat flux (Fig. 8b) tended to be similar. This feature will undoubtedly enhance the risk of hazardous events in urban environments and increase the difficulty of mitigating the UHI effect at night.

3.3. *Impacts of heat waves on urban warming*

To explore the impacts of heat waves or high temperature weather on summer urban warming, we present the temporal evolution of the change in daily, daytime and nighttime mean temperature over the six-ring area of Beijing (Fig. 9). Clearly, no drastic fluctuation in daytime average warming occurred in HW or on other simulated high-temperature days (Fig. 9b). Statistical testing also indicated that the daytime-averaged warming had no correlation with daily maximum temperature ($P > 0.05$). However, a larger daytime-averaged warming was apparent in August (Fig. 9b), subsequently leading to a larger daily mean warming in August (Fig. 9a). This is consistent with the result reported by Cao et al. (2016) regarding summer temporal evolution (significant urban warming in August in the BTH region).

The nocturnal warming generally changed with the daily maximum air temperature ($P < 0.05$; Fig. 9c), indicating heat waves may intensify urban-induced warming at night. However, the heat wave intensity cannot indicate the magnitude

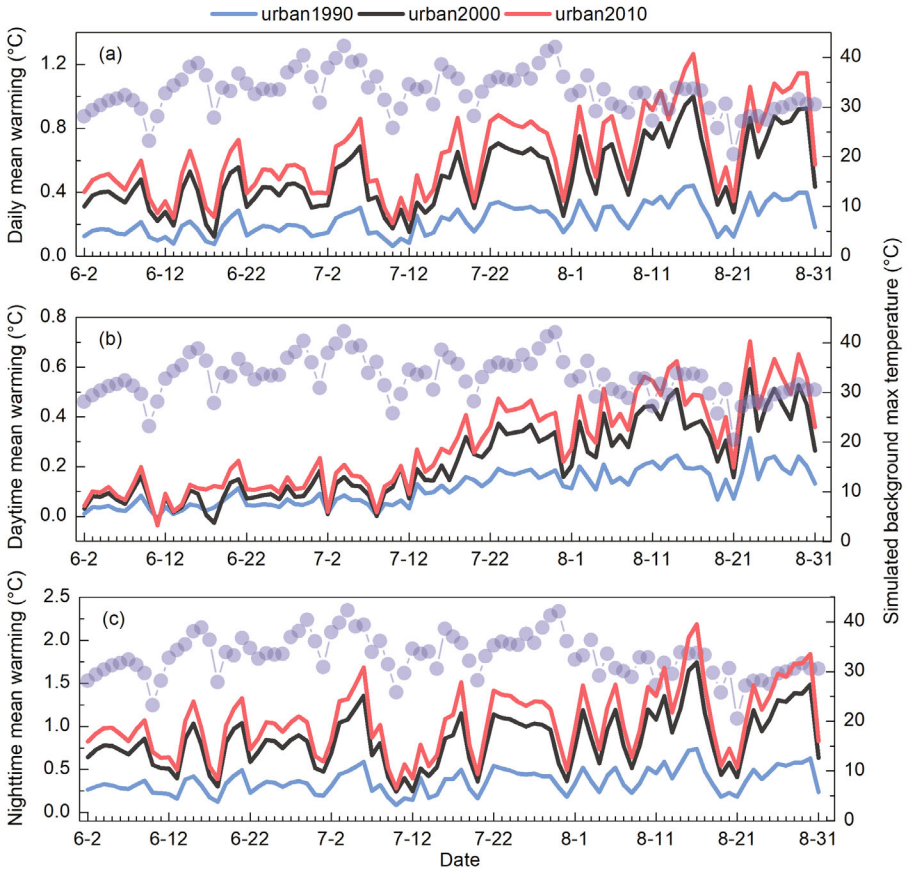

Fig. 9. Time series of urban-induced change in (a) daily, (b) daytime (0700–1900 LST) and (c) nighttime (2000–0600 LST) mean 2-m air temperature averaged over the six-ring area between the three urban development periods [urban1990 (blue line), urban2000 (black line) and urban2010 (red line)] and the crop scenario (left-hand *y*-axis). The line and symbol plot represents the time series of the simulated maximum 2-m air temperature averaged over the six-ring area for the crop scenario (right-hand *y*-axis).

of urban warming (the correlation coefficient between nighttime mean warming and daily maximum temperature was 0.25); for example, warming intensities during 29–30 July were not very high during JJA, although there were the higher daily maximum temperatures during 29–30 July compared to other days in JJA (Fig. 9c). The stronger urban warming at night was caused by more daytime stored heat, which resulted from the stronger solar radiation during the day. Also, it was generally cloudless on high-temperature days, which provided stronger solar radiation. In fact, heat waves or high-temperature days result from all kinds of forcing factors in addition to urban warming (e.g., warm advection, local thermal dynamic processes), so the change in warming intensity caused by heat waves may be influenced by other climate factors, leading to a weak correlation between nighttime mean warming and daily maximum temperature.

Although daily mean warming correlated with the daily maximum temperature due to the feature of nighttime warming, the correlation was not significant ($P > 0.05$) because of the contribution of daytime mean warming (higher warming in August). Wang et al. (2017a) indicated that the summer urban warming intensities were strengthened during the extreme heat period over the Yangtze River Delta (YRD) region. This was because of no obvious daytime mean warming in August in the YRD region. Moreover, Cao et al. (2016) showed more obvious daily mean warming in August occurring in the BTH than the YRD and Pearl River Delta regions. Figure 9 also shows that the daily (daytime and nighttime) mean warming intensity in summer in Beijing markedly increased with urban expansion during 1990–2010.

We explain the phenomenon based on the surface energy balance. Figure 10 shows the time series of the changes in daily, daytime and nighttime mean surface heat fluxes averaged over the six-ring area between urban2010 and the crop scenario. The temporal evolution of the urban warming was directly related to the temporal variation of the changes in sensible heat flux (Fig. 10a). Clearly, the change in latent heat flux, as shown by the daytime average, increased markedly from late July on (Fig. 10b). It led to a significant increase in sensible heat flux during the daytime (Fig. 10a) and, accordingly, the increase in urban warming in August (Fig. 9b). Statistical testing also indicated that the change in sensible heat flux had a significant negative correlation with the change in latent heat flux during the daytime ($R = -0.894$; $P < 0.01$). Figure 11 shows the daily mean precipitation simulated by the urban2010 run averaged over the six-ring area in Beijing.

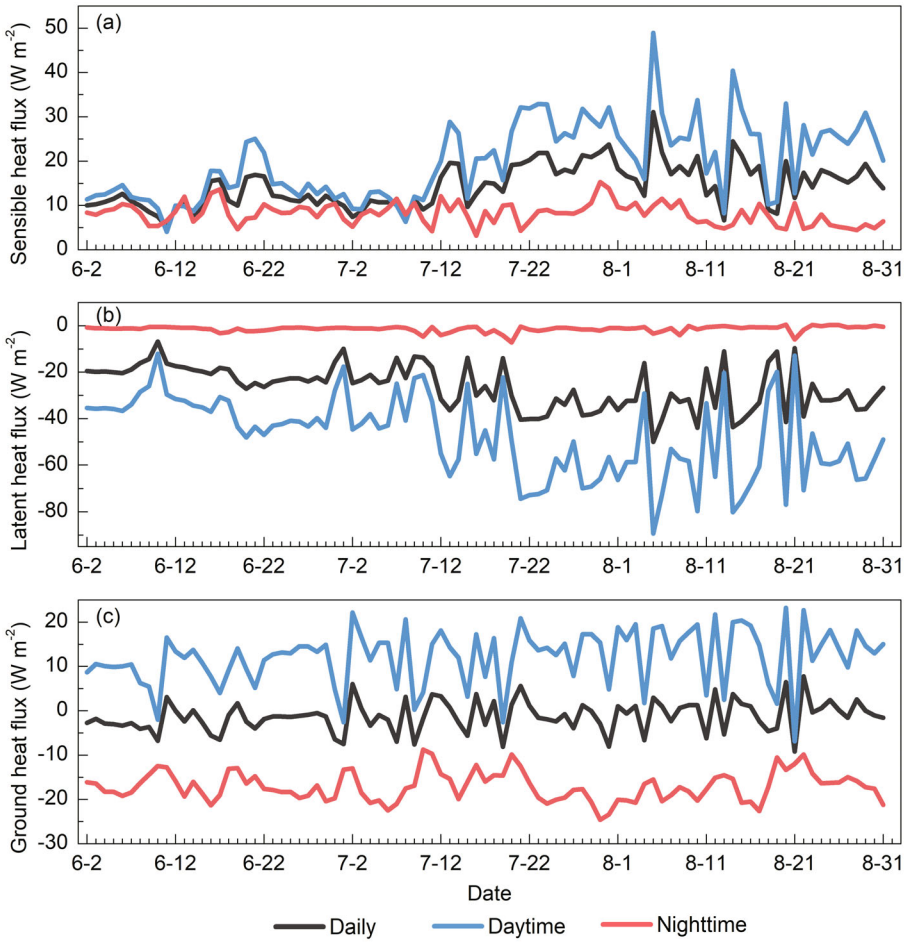

Fig. 10. Time series of the change in daily (black line), daytime (blue line) and nighttime (red line) mean (a) sensible heat flux, (b) latent heat flux and (c) ground heat flux averaged over the six-ring area between urban2010 and the crop scenario.

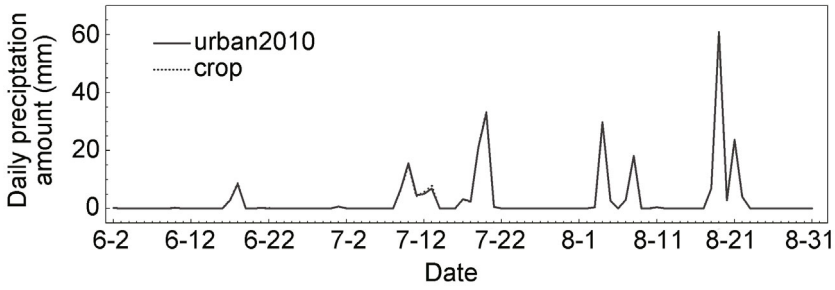

Fig. 11. Daily mean precipitation simulated by the urban2010 and crop runs averaged over the six-ring area of Beijing.

It indicates that the precipitation increased from late July on in urban and crop areas. The soil moisture in the crop areas increased markedly, while that in urban areas increased slightly due to the impervious surfaces and drainage systems in these areas. Thus, the difference in water evaporation between the urban and crop surfaces increased, further leading to the greater urban-induced change in latent heat flux in August in Beijing (Fig. 10b). More heat was stored in the urban surface during the day, leading to a greater heat release at night. The changes in nighttime air temperature were primarily attributable to the alterations in ground heat flux, because the changes in latent heat flux at night were close to zero. The heat wave and other high temperature days caused more heat to be stored in the surface during the daytime, a greater heat release at night, and thus the larger nighttime warming. Previous studies have demonstrated a positive correlation between ground heat flux and surface net radiation, especially for concrete surfaces (Bai, 2015). In general, it was cloudless on the high-temperature days, providing stronger solar radiation and then more ground heat flux during the day.

Heat waves are induced by large-scale, stagnant, high pressure systems that produce a temporal temperature anomaly for a region (Li and Bou-Zeid, 2013); and they are the end result of all kinds of forcing factors, such as warm advection and local thermodynamic processes. Heat waves can increase the surface air temperature over both urban and crop areas. Our results indicate that heat waves enhance the nocturnal urban warming in summer in Beijing and further cause a change in daily mean warming to some extent. That is, heat waves induce a higher increment of air temperature in urban areas than in crop areas. This implies that urban land expansion may heighten heat waves in urban areas. Therefore, urban-induced warming should be considered as one possible source of heat waves in urban areas.

4. Conclusion

This study began by examining the influences of urban land expansion in Beijing on the near-surface temperature in summer. We used three land use datasets and a hypothetical crop scenario to simulate the evolution of urban warming caused by different periods of urban expansion during 1990–2010, and discussed the mechanism based on the surface energy balance. Based on the simulated results, we further analyzed the impacts of a heat wave and other high-temperature days on urban-induced warming, and explored the mutual relationship between urban-induced warming and heat waves. The main conclusions are:

(1) The urban warming area expanded at approximately the same scale as the urban land expansion during 1990–2010. The summertime mean urban warming in the 1990, 2000 and 2010 urbanization periods was 0.23°C, 0.50°C and 0.64°C, respectively, averaged over the six-ring area of Beijing. Urban warming increased with urban land expansion, but the speed of warming slowed slightly during 2000–2010. The diurnal cycle of urban warming showed the smallest warming occurring at 1200 LST, and it peaking at around 2000 LST. In the day, a significant decrease in latent heat flux in urban areas resulted in more sensible heat flux from the urban surface layer to the air, leading to daytime warming. At night, the release of stored heat led to a small increase in sensible heat flux. Urban warming at night was higher than that in the day, although the nighttime increment in sensible heat flux was smaller. This was because the surface heat was not easily released in urban areas under the stable PBL stratification at night. Moreover, the large amounts of storage and slow release of urban heat may have caused the larger nighttime longwave radiation in urban areas, and thus the greater urban warming at night.

(2) A heat wave and high temperature weather enhanced the urban warming intensity at night. Also, statistical testing indicated a significant positive relationship between daily maximum temperature and nocturnal urban warming. The reason was that the larger amounts of heat stored in the urban surface during the daytime of the heat wave or high temperature days caused a larger heat release at night, thus leading to the greater urban warming at night. Heat waves may induce a larger increment of air temperature in urban areas than in crop areas. That is, urban land expansion may strengthen the intensity of heat waves in urban areas. Therefore, there is a positive feedback effect between urban warming and heat waves in urban areas.

Acknowledgements. This work was supported by the National Basic Research Program of China (Grant No. 2015CB953602) and the National Social Science Fund of China (Grant No. 17BGL256).

REFERENCES

Bai, G. Q., 2015: Simulation on the temperature and thermal flux about two kinds of surface layers. M.S. thesis, Nanjing University of Information Science & Technology. (in Chinese)

Cao, Q., D. Y. Yu, M. Georgescu, and J. G. Wu, 2016: Impacts of urbanization on summer climate in China: An assessment with coupled land-atmospheric modeling. *J. Geophys. Res. Atmos*., **121**, 10 505–10 521, https://doi.org/10.1002/2016JD025210.

Chen, F., and J. Dudhia, 2001: Coupling an advanced land surface–hydrology model with the Penn State–NCAR MM5 modeling system. Part I: Model implementation and sensitivity. *Mon. Wea. Rev*., 569–585, https://doi.org/10.1175/1520-0493(2001)129<0569:CAALSH>2.0.CO;2.

Chen, F., X. C. Yang, and W. P. Zhu, 2014: WRF simulations of urban heat island under hot-weather synoptic conditions: The case study of Hangzhou City, China. *Atmospheric Research*, **138**, 364–377, https://doi.org/10.1016/j.atmosres.2013.12.005.

Chen, F., H. Kusaka, M. Tewari, J. W. Bao, and H. Hirakuchi, 2004: Utilizing the coupled WRF/LSM/urban modeling system with detailed urban classification to simulate the urban heat island phenomena over the greater Houston area. *Proc. 5th Symposium on the Urban Environment*, American Meteorological Society, Vancouver, BC, Canada.

Chen, J., 2007: Rapid urbanization in China: A real challenge to soil protection and food security. *Catena*, **69**, 1–15, https://doi.org/10.1016/j.catena.2006.04.019.

Cui, Y. P., J. Y. Liu, X. Z. Zhang, Y. C. Qin, and J. W. Dong, 2015: Modeling urban sprawl effects on regional warming in Beijing-Tianjing-Tangshan urban agglomeration. *Acta Ecologica Sinica*, **35**, 993–1003, https://doi.org/10.5846/stxb201305191114. (in Chinese)

Douglas, E. M., D. Niyogi, S. Frolking, J. B. Yeluripati, R. A. Pielke, N. Niyogi, C. J. Vörösmarty, and U. C. Mohanty, 2006: Changes in moisture and energy fluxes due to agricultural land use and irrigation in the Indian Monsoon Belt. *Geophys. Res. Lett*., **33**, L14403, https://doi.org/10.1029/2006GL026550.

Dudhia, J., 1989: Numerical study of convection observed during the winter monsoon experiment using a mesoscale two-dimensional model. *J. Atmos. Sci*., **46**, 3077–3107, https://doi.org/10.1175/1520-0469(1989)046<3077:NSOCOD>2.0.CO;2.

Fang, C. L., G. D. Li, and S. J. Wang, 2016: Changing and differentiated urban landscape in China: Spatiotemporal patterns and driving forces. *Environ. Sci. Technol*., **50**, 2217–2227, https://doi.org/10.1021/acs.est.5b05198.

Feng, J. M., J. Wang, and Z. W. Yan, 2014: New advances in the research of climatic effect of urbanization. *Advances in Meteorological Science and Technology*, **4**, 21–29, https://doi.org/10.3969/j.issn.2095-1973.2014.05.002. (in Chinese)

Feng, J. M., Y. L. Wang, Z. G. Ma, and Y. H. Liu, 2012: Simulating the regional impacts of urbanization and anthropogenic heat release on climate across China. *J. Climate*, **25**, 7187–7203, https://doi.org/10.1175/JCLI-D-11-00333.1.

Field, C. B., and Coauthors, 2012: *Managing the Risks of Extreme Events and Disasters to Advance Climate Change Adaptation. Special Report of the Intergovernmental Panel on Climate Change*. Cambridge University Press.

Hales, S., 2015: *Quantitative Risk Assessment of the Effects of Climate Change on Selected Causes of Death, 2030s and 2050s*. World Health Organization, Geneva.

Hong, S. Y., J. Dudhia, and S. H. Chen, 2004: A revised approach to ice microphysical processes for the bulk parameterization of clouds and precipitation. *Mon. Wea. Rev*., **132**, 103–120, https://doi.org/10.1175/1520-0493(2004)132<0103:ARATIM>2.0.CO;2.

Hong, S. Y., Y. Noh, and J. Dudhia, 2006: A new vertical diffusion package with an explicit treatment of entrainment processes. *Mon. Wea. Rev*., **134**, 2318–2341, https://doi.org/10.1175/MWR3199.1.

Jacobson, M. Z., S. V. Nghiem, A. Sorichetta, and N. Whitney, 2015: Ring of impact from the mega-urbanization of Beijing between 2000 and 2009. *J. Geophys. Res. Atmos*., **120**, 5740–5756, https://doi.org/10.1002/2014JD023008.

Kain, J. S., 2004: The Kain-Fritsch convective parameterization: An update. *J. Appl. Meteor*., **43**, 170–181, https://doi.org/10.1175/1520-0450(2004)043<0170:TKCPAU>2.0.CO;2.

Kalnay, E., and M. Cai, 2003: Impact of urbanization and land-use change on climate. *Nature*, **423**, 528–531, https://doi.org/10.1038/nature01675.

King, D., D. Schrag, D. D. Zhou, Q. Ye, and A. Ghosh, 2015: *Climate Change: A Risk Assessment*. Centre for Science and Policy.

Kusaka, H., and F. Kimura, 2004: Thermal effects of urban canyon structure on the nocturnal heat island: Numerical experiment using a mesoscale model coupled with an urban canopy model. *J. Appl. Meteor*., **43**, 1899–1910, https://doi.org/10.1175/JAM2169.1.

Kusaka, H., F. Chen, M. Tewari, J. Dudhia, D. O. Gill, M. G. Duda, W. Wang, and Y. Miya, 2012: Numerical simulation of urban heat island effect by the WRF model with 4-km grid increment: An inter-comparison study between the urban canopy model and slab model. *Journal of the Meteorological Society of Japan*, **90B**, 33–45, https://doi.org/10.2151/jmsj.2012-B03.

Kusaka, H., H. Kondo, Y. Kikegawa, and F. Kimura, 2001: A simple single-layer urban canopy model for atmospheric models: Comparison with multi-layer and slab models. *Bound.-Layer Meteor*., **101**, 329–358, https://doi.org/10.1023/A:1019207923078.

Li, D., and Bou-Zeid, E., 2013: Synergistic interactions between urban heat islands and heat waves: the impact in cities is larger than the sum of its parts. *Journal of Applied Meteorology and Climatology*, **52**, 2051–2064, https://doi.org/10.1175/ JAMC-D-13-02.1.

Meng, W. G., Y. X. Zhang, J. N. Li, W. S. Lin, G. F. Dai, and H. R. Li, 2011: Application of WRF/UCM in the simulation of a heat wave event and urban heat island around Guangzhou. *Journal of Tropical Meteorology*, **17**, 257–267, https://doi.org/10.3969/j.issn.1006-8775.2011.03.007.

Miao, S. G., F. Chen, M. A. LeMone, M. Tewari, Q. C. Li, and Y. C. Wang, 2009: An observational and modeling study of characteristics of urban heat island and boundary layer structures in Beijing. *Journal of Applied Meteorology and Climatology*, **48**, 484–501, https://doi.org/10.1175/2008JAMC1909.1.

Mlawer, E. J., S. J. Taubman, P. D. Brown, M. J. Iacono, and S. A. Clough, 1997: Radiative transfer for inhomogeneous atmospheres: RRTM, a validated correlated-k model for the longwave. *J. Geophys. Res.*, **102**, 16 663–16 682, https://doi.org/10.1029/97JD00237.

National Bureau of Statistics PRC, 2014: *China Statistical Year-*

book. China Statistics Press. (in Chinese)

Oke, T. R., 1982: The energetic basis of the urban heat island. *Quart. J. Roy. Meteor. Soc*., **108**, 1–24, https://doi.org/10.1002/qj.49710845502.

Skamarock, W. C., and Coauthors, 2008: A description of the advanced research WRF version 3. NCAR Technical Note, NCAR/TN-475+STR, https://doi.org/10.5065/D68S4MVH.

Stott, P. A., D. A. Stone, and M. R. Allen, 2004: Human contribution to the European heatwave of 2003. *Nature*, **432**, 610–614, https://doi.org/10.1038/nature03089.

Sun, Y., X. B. Zhang, F. W. Zwiers, L. C. Song, H. Wan, T. Hu, Y. Hong, and G. Y. Ren, 2014: Rapid increase in the risk of extreme summer heat in Eastern China. *Nat. Clim. Change*, **4**, 1082–1085, https://doi.org/10.1038/nclimate2410.

Sun, Y., X. B. Zhang, G. Y. Ren, F. W. Zwiers, and T. Hu, 2016: Contribution of urbanization to warming in China. *Nat. Clim. Change*, **6**, 706–709, https://doi.org/10.1038/nclimate2956.

Tewari, M., F. Chen, H. Kusaka, and S. G. Miao, 2007: Coupled WRF/Unified Noah/Urban-canopy modeling system. Ncar WRF Documentation, NCAR, Boulder.

Wang, J., J. M. Feng, and Z. W. Yan, 2015a: Potential sensitivity of warm season precipitation to urbanization extents: Modeling study in Beijing-Tianjin-Hebei urban agglomeration in China. *J. Geophys. Res. Atmos*., **120**, 9408–9425, https://doi.org/10.1002/2015JD023572.

Wang, J., Z. W. Yan, X. W. Quan, and J. M. Feng, 2017a: Urban warming in the 2013 summer heat wave in eastern China. *Climate Dyn*., **48**, 3015–3033, https://doi.org/10.1007/s00382-016-3248-7.

Wang, J., J. M. Feng, Z. W. Yan, Y. H. Hu, and G. S. Jia, 2012: Nested high-resolution modeling of the impact of urbanization on regional climate in three vast urban agglomerations in China. *J. Geophys. Res.*, **117**, https://doi.org/10.1029/2012JD018226.

Wang, J., Z. W. Yan, Z. Li, W. D. Liu, and Y. C. Wang, 2013a: Impact of urbanization on changes in temperature extremes in Beijing during 1978-2008. *Chinese Science Bulletin*, **58**, 4679–4686, https://doi.org/10.1007/s11434-013-5976-y.

Wang, K. C., S. J. Jiang, J. K. Wang, C. L. Zhou, X. Y. Wang, and X. Lee, 2017b: Comparing the diurnal and seasonal variabilities of atmospheric and surface urban heat islands based on the Beijing urban meteorological network. *J. Geophys. Res. Atmos*., **122**, 2131–2154, https://doi.org/10.1002/2016JD025304.

Wang, M. N., X. D. Yan, J. Y. Liu, and X. Z. Zhang, 2013b: The contribution of urbanization to recent extreme heat events and a potential mitigation strategy in the Beijing–Tianjin–Hebei metropolitan area. *Theor. Appl. Climatol*., **114**, 407–416, https://doi.org/10.1007/s00704-013-0852-x.

Wang, X. M., X. G. Sun, J. P. Tang, and X. Q. Yang, 2015b: Urbanization-induced regional warming in Yangtze River Delta: Potential role of anthropogenic heat release. *International Journal of Climatology*, **35**, 4417–4430, https://doi.org/10.1002/joc.4296.

Xie, Z., and H. X. Cao, 1996: Asymmetric changes in maximum and minimum temperature in Beijing. *Theor. Appl. Climatol*., **55**, 151–156, https://doi.org/10.1007/BF00864710.

Yan, Z. W., Z. Li, Q. X. Li, and P. Jones, 2010: Effects of site change and urbanisation in the Beijing temperature series 1977-2006. *International Journal of Climatology*, **30**, 1226–1234, https://doi.org/10.1002/joc.1971.

Zhang, N., L. F. Zhu, and Y. Zhu, 2011: Urban heat island and boundary layer structures under hot weather synoptic conditions: A case study of Suzhou city, China. *Adv. Atmos. Sci*., **28**, 855–865, https://doi.org/10.1007/s00376-010-0040-1.

Zhou, L. M., R.E. Dickinson, Y. H. Tian, J. Y. Fang, Q. X. Li, R. K. Kaufmann, C. J. Tucker, and R. B. Myneni, 2004: Evidence for a significant urbanization effect on climate in China. *Proceedings of the National Academy of Sciences of the United States of America*, **101**, 9540–9544, https://doi.org/10.1073/pnas.0400357101.